Hindawi
Advances in Materials Science and Engineering
Volume 2019, Article ID 8715718, 8 pages
https://doi.org/10.1155/2019/8715718

Research Article

Mini-Extruder for 3D Magnetoactive Polymer Printing

Nina Prem, Dirk Sindersberger, and Gareth J. Monkman

Faculty of Electrical Engineering and Information Technology, Mechatronic Research Unit, OTH Regensburg, Germany

Correspondence should be addressed to Gareth J. Monkman; gareth.monkman@oth-regensburg.de

Received 28 November 2018; Revised 4 May 2019; Accepted 7 May 2019; Published 30 May 2019

Academic Editor: Peter Majewski

This work describes the development of a new miniature extruder, essential to cavity-free 3D printing of silicone-based smart materials. This makes the 3D printing of magnetoactive and electroactive polymer soft robotic components and devices directly from CAD data possible. The special feature of such an extruder is that it is designed for use with addition-crosslinking RTV-2 silicones, including solid particulate additives. The extruder merges the respective components automatically during extrusion which obviates the need for premixing and vacuum evacuation. Problems associated with inhomogeneities and unwanted cavity production are consequently eliminated. Rheological details necessary to the design, together with some preliminary performance results, are presented.

1. Introduction

Additive manufacturing, otherwise known as "3D printing," describes a process in which a component based on digital 3D design data is manufactured through layer-by-layer structuring of a material [1, 2].

Smart materials exhibit parametric changes resulting from external stimuli such as thermal, magnetic or electric fields, mechanical loads, or changes in pH value or humidity [3]. These often require an active supply of energy [4], as in the case of piezoelectric and electrostrictive materials, functional fluids, shape memory alloys, and polymers. For the purposes of sensing, control, and actuation, smart materials are used to design smart structures and devices [5].

Elastomeric materials such as magnetoactive polymers (MAPs) and electroactive polymers (EAPs) represent some of the most recent forms of smart composites to be developed. MAPs consist of a polymer matrix, typically an elastomer, in which magnetic particles such as carbonyl iron powder (CIP) are embedded by means of specific manufacturing processes [6]. As a result, their mechanical and magnetic properties are coupled with one another [7]. In a similar manner, electroactive polymers (EAPs) may contain additional dielectric particles [8] and in some cases electrically conductive particles [9]. The 3D printing of thermoplastic polymers is an established technology. The extension to silicones is somewhat newer, and 3D printing systems, which permit the inclusion of different ferromagnetic and/or ferroelectric materials, are currently not yet commercially available. Such a system would increase fabrication repeatability whilst minimizing time and material consumption.

In order to achieve this, the mixing and cavity-free extrusion of viscous compounds is required. For small-scale fabrication, problems associated with rapid vulcanization are somewhat mitigated, but no such microextruder exists commercially. The simple scaling down of larger sized industrial extruders is technically difficult as the rheological factors effecting extrusion are highly dependent on specific dimensions. The objective of this work is the development and fabrication of a microextruder prototype for the automated cavity-free 3D printing of MAP and EAP elements.

In addition, the system can be enhanced for 6D printing where graduated diffusion of particle distribution and orientation isotropy are necessary [10].

2. Materials

Throughout this work, two component addition-curing RTV-2 silicones are utilized. One component contains the polymer and the crosslinker, while the other component includes the polymer and a platinum catalyst. Vulcanization commences on the contact between crosslinker and catalyst. During the

mixing of the two components A and B under normal atmospheric conditions, a certain amount of air is inevitably trapped within the mixture. To achieve completely cavity-free mixtures, the compounds must be degassed (evacuated) under reduced pressure (10–20 mbar) in a desiccator or vacuum oven.

The rate and degree of cavity generation depends largely on the mixing method and the additives involved. Cavity sizes are typically in the order of 80 μm to 120 μm diameter with rising velocities typically of the order of 0.1 m/s through medium with a dynamic viscosity of $\mu = 1500$ mPa·s at 23° (polymer prior to curing). These results in a Reynolds factor much lower than 1 thus ensure laminar flow [11]. In contrast to condensation-curing RTV-2 silicones, the vulcanization speed is controlled exclusively by temperature. Furthermore, no secondary products are generated, and weight loss during vulcanization is not possible resulting in a very low shrinkage rate.

Particles may be embedded into the polymer matrix at any stage prior to vulcanization. A distinction is made here between magnetic, dielectric, and electrically conductive particles. Due to the interaction of magnetic particles embedded in an elastic polymer matrix, the mechanical and magnetic properties are coupled with each other and reversibly influenced by external stimuli such as a magnetic field or temperature [12]. The particles may be magnetically soft (CIP), hard (NdFeB), or bimodal [7]. The application of an external magnetic field causes temporary magnetization of soft magnetic particles resulting in particle-particle and particle-matrix interactions [13], whereas MAP containing hard magnetic particles may be permanently magnetized [14]. In addition to magnetic particles, electrically conductive particles such as graphite, aluminium graphite, or carbon black may be included. High-permittivity particles may also be included in combination with RTV-2 silicone [8].

In addition to the difficulties associated with 3D printing of silicones, the integration of particles into the mixture is another challenge. Excessive particulate can lead to the mixture being no longer 3D printable. This depends on the particles used (carbon black, graphite, aluminium graphite, etc.) [9]. In contrast to inert fillers such as chalk, kaolin, or aluminium oxide hydrate, active filler particles such as carbon black interact with the rubber matrix. Inert fillers dilute the matrix and primarily serve to reduce costs and weight. However, active fillers change the viscoelastic properties through interaction with the matrix. Interactions between the carbon black network and the bonds between rubber and carbon black are based on van der Waals forces-two-pole-dipole interactions between hydrogen bonds [15]. The physical bonding of carbon black to the polymer reduces chain mobility, and thus both the viscoelasticity of the polymer and the elongation of the chain properties increase [15]. The advantage of 3D MAP and EAP printing is that elastic, conductive, and/or magnetic elements can be integrated into components with higher precision than those that are possible with simple moulding.

3. Rheology and Flow

In order to develop the necessary microextruder, the rheological behavior of the materials and their flow properties must be understood. Viscoelastic fluid mechanical properties such as deformation and transient flow behavior of the media must be described.

3.1. Structural Viscosity and Shear Rate. In the non-crosslinked state, silicone base and catalyst are viscous fluids. Viscoelasticity increases during crosslinking, and the final crosslinked silicones are elastic with a wide range of Young's moduli (1 Pa–100 kPa) [16]. Consequently, a transition from a liquid to an elastic solid state takes place during the crosslinking process. The viscoelastic character of the liquid is strongly dependent on the deformation time. Previous studies have shown that the silicone polymer always returns elastically on reduction of the deformation force [17]. Generally, most silicones are referred to as structurally viscous prior to curing. Dynamic viscosity η (Pa·s) is a measure of the resistance to flow of a medium. Synthetic materials can have very high viscosities resulting in correspondingly high flow resistance. Due to the high viscosity of these materials, significant pressure is required to inject the material into a mould. For Newtonian media, the viscosity η is a pure material property and depends only on pressure and temperature. In the case of structurally viscous media, η is influenced by the deformation rate. This implies that the viscosity η of such a medium decreases with increasing shear rate (flow velocity). In contrast, by reason of the structural viscosity of the liquid, the viscosity η increases again with decreasing shear rate until (theoretically) zero viscosity $\eta 0$ is reached. A further reduction of the shear rate does not lead to a further increase in η. Structural viscosity is explained as follows: synthetic materials are macromolecules in the form of chains. At rest, the macromolecules attempt to achieve the greatest possible entropy and are thus disordered with the molecular chains entangled. As a result, considerable energy is initially required to move this macromolecular structure, i.e., to generate flow. The flow process causes the individual layers of the liquid to move relative to one another. As a consequence of this process, shear stresses are transmitted between the layers due to internal friction (dissipation) [17]. These shear stresses influence the individual molecular chains causing alignment of the disordered chains in the direction of flow. The more the molecular chains are stretched, i.e., aligned, the less the energy is required to cause them to slide past each other. For this reason, the viscosity decreases with increasing shear rate. If the molecular orientation becomes more pronounced, the energy required to cause flow again increases. As the viscosity rises at very high shear rates, the polymer molecules are brought out of their most energetically favorable positions and these effects are no longer significant. Restoring forces are formed, as a result of which the polymer endeavors to return to the state of greatest possible entropy. In turn, these restoring forces counteract the shear forces in order to maintain equilibrium. This is dependent on the strength of the molecular orientation/alignment and the temperature. High temperature results in high activation energy and thus high restoring forces.

3.2. Memory and Deformation Times. It should be noted that a memory time can be assigned to the raw mixture of the

silicone [17]. This is described as the time required to form or dissolve long and entwined macromolecule chains. Now the question arises as to the typical deformation time in the processing of silicones. Two adjacent elastomer particles moving in parallel paths along a wall at a distance Δy, speed u, and $u + \Delta u$ are separated from one another. Consequently, the gravitational angle, caused by $y = \Delta u t/\Delta y$, grows indefinitely, but the temporal change in the shear angle, the shear rate $\dot{\gamma} = \Delta u/\Delta y$, remains constant. If the particles now flow near the axis of symmetry, the velocity difference Δu is small resulting in a low shear rate $\dot{\gamma}$, and in the center of a capillary, the shear rate is zero. In general, viscous fluids tend to adhere to walls. As a result, the shear rate along the wall is at its maximum. It is not difficult to calculate the order of magnitude of the shear rate along the cannula walls [17]:

$$\dot{\gamma} = \frac{U}{d}. \tag{1}$$

The cannula used in this work has a diameter of 1.5 mm and an average flow velocity of about 0.15 m/s which gives a shear rate of $100\,s^{-1}$.

If the deformation time is now much longer than the molecular memory time, it will be sufficient to loosen the entanglements, i.e., the elastic part of the module is small. This molecular memory effect is responsible for some important phenomena in the manufacturing process, e.g., normal stresses, swelling during extrusion, and expansion pressure losses during flow due to reduction in conduit cross section and wall slippage.

3.3. Impact of Temperature. If the temperature in the extruder is high enough to activate the crosslinking reaction, the network prevents the molecules from sliding as the degree of crosslinking increases. If the shear amplitude remains unchanged, the shear stress in the material increases and thus also the measured torque. However, at the same time, the phase angle δ between shear and direct stress decreases. The typical course of events for throughput as a function of time when using a vibrating rheometer is described by Pelz [17], illustrated in Figure 1.

At a given temperature, the speed of the crosslinking reaction can be determined by evaluation of the throughput curve. However, the temperature of an elastomer particle does not remain constant over time and each particle has its own local temperature-time characteristic. Increase in torque M is directly proportional to the crosslinking density, i.e., the number of crosslinking locations per unit volume. Theoretically, it is now possible to calculate the energy dissipation against time, which can be utilized to determine the speed of the crosslinking reaction at a given temperature. Table 1 contains the values for the crosslinking time with the corresponding temperatures for the silicones used in this work:

$$\alpha = \frac{M(t) - M_{\min}}{M_{\max} - M_{\min}} = \frac{\text{crosslinking density}}{\text{max crosslinking density}}. \tag{2}$$

A further phenomenon can be observed with structurally viscous liquids. Under shear loading, the liquid attempts to move perpendicularly to the direction of force, i.e., shear direction.

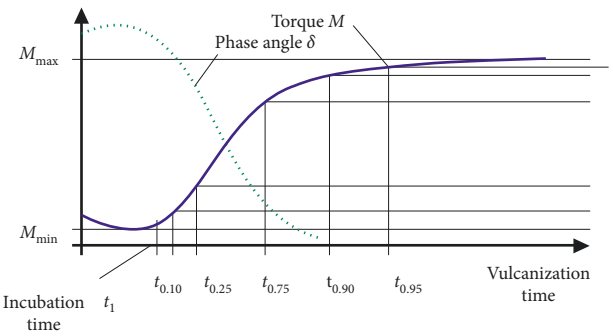

Figure 1: Typical torque M and phase angle δ curve at constant temperature for an elastomer compound [17].

Table 1: Crosslinking time as a function of temperature, SF00 and SF13 (Silikonfabrik).

RTV-2 silicone SF00		RTV-2 silicone SF13
Temperature	Crosslinking time	Temperature
<10°C	The crosslinking process is almost nonexistent	<10°C
~23°C	1.5 h[1]	~23°C
~50°C	Ca. 15 min[1]	~50°C
~150°C	Ca. 30 sec[1]	~150°C

[1]Depending on the thickness of the sample.

4. Effects of Dissipation

During processing, the raw mixture of silicone is subjected to shear stress. As already described, shearing leads to a frictional process between the individual layers of liquid. This frictional process between the molecular chains is called dissipation, which results in heating of the medium. The energy equation is as follows [18]:

$$\rho C_p \left(\frac{\delta\theta}{\delta t} + v_x \frac{\delta\theta}{\delta x} \right) = \left(\lambda \frac{\delta\theta}{\delta y} - \tau_{xy} \frac{\delta v_x}{\delta y} \right). \tag{3}$$

If the heat conduction (adiabatic process) and the heat transport in the flow direction are neglected, the relevant parameters in expression (3) can be repeated in the following simplified forms:

$$\rho C_p \frac{\delta\theta}{\delta t} = -\tau_{xy} \frac{\delta v_x}{\delta y},$$

$$\text{with } \tau = \eta\dot{\gamma}, \tag{4}$$

$$\frac{\delta v_x}{\delta y} = \dot{\gamma},$$

$$\rho C_p \frac{\delta\theta}{\delta t} = -\eta\dot{\gamma} \longrightarrow -\Delta\theta = \frac{1}{\rho C_P} \eta\dot{\gamma}^2 \Delta t, \tag{5}$$

$$\frac{\delta v_x}{\delta y} = \dot{\gamma}.$$

Equations (4) and (5) illustrate how the development of heat in the medium is strongly dependent on the shear rate. Consequently, if the shear rate is very high (boundary layers),

a high thermal dissipation results and heat is generated. Since the viscosity is also a function of temperature, the viscosity will increase due to the higher temperature in the boundary layers. In accordance with the first law of thermodynamics,

$$dU + dE_a = \delta Q + \delta W. \tag{6}$$

If the process is adiabatic, then

$$\Delta p \dot{V} = m C_p \Delta\theta. \tag{7}$$

The simplified relationship between temperature increases due to raising pressure, which is given as follows:

$$\Delta\theta \propto \frac{1}{\left(\rho c_p\right)} \Delta p, \quad \text{with } m = \rho V. \tag{8}$$

From this, a rough estimate of the change in temperature as a function of pressure can be derived.

5. Normal Stress

If the media demonstrate viscoelastic flow behavior, as do silicones, shear forces causes normal strains in addition to shear strains. These strains run perpendicular to the direction of shear stress and are present on all surfaces of the volume element in the viscoelastic media. In practice, a distinction must be made between shear stresses in the direction of flow and normal stresses perpendicular to the direction of flow. The occurrence of normal stresses can lead to certain effects. The Weissenberg effect or rod climb effect describes the behavior of viscoelastic liquids under shear strain rates and relatively low temperature. If a rotating rod is placed in a vessel containing a viscoelastic fluid, normal stress is generated and in particular, tensile stress in the direction of flow. If this force effect is greater than the radial acceleration acting in the opposite direction, material accumulates and the liquid level rises in the direction of the axis of rotation (rotating rod). The quality of the flow depends on the dominance of the radial acceleration or the normal stresses. Furthermore, the pressure and flow conditions change in such apparatus. In a viscoelastic liquid, the rotating rod in the center of the vessel leads to a pressure gradient between the center and the edge. This behavior can be helpful in the development of an extruder. Considering a fluid jet passing out through a circular, vertical tube (e.g., a cannula), it is possible to determine a number of parameters. In a viscoelastic medium, gravity causes the fluid to accelerate and thus the velocity increases as the distance from the outlet increases. In addition, the shear deformation near the outlet causes a tensile stress in the direction of flow and a compressive stress (normal stress) in the transverse direction. This leads to an expansion of the jet compared to the nozzle diameter. This effect is also referred to as strand or extrudate threshold and the resulting strand shape as onion formation [18]. This effect becomes more pronounced the smaller the nozzle dimensions and the higher the flow velocity. In this work, the cannula has a diameter $d = 1.5$ mm and length $l = 10$ mm. This must be taken into account as the strand expansion is stronger at the center between the wall surfaces than it is in the corners where the velocity gradients and thus the elastic deformation are lower. One solution is modification of the nozzle geometry.

6. Calculation of Design Parameters

In order to obtain an approximation for the design and construction of the extruder, it is necessary to consider thermodynamics and fluid mechanics for which a few assumptions must be made:

(i) The medium is incompressible
(ii) Laminar flow prevails
(iii) Wall adhesion
(iv) Acceleration and gravitational forces are neglected
(v) Isothermal conditions
(vi) Validity of temporally and locally averaged conservation equations

With the help of these simplifications and using the mass and momentum conservation, Hagen–Poiseuille's law for a cylindrical conduit geometry can be derived [19]. With addition of the continuity equation, the volumetric flow rate $\dot{V}$ for a conduit of radius r and length l can be obtained as follows:

$$\dot{V} = \frac{\partial V}{\partial t} = \frac{\pi r^4 \Delta p}{8\eta l}. \tag{9}$$

What is often required is the pressure gradient in the conduit, Δp:

$$\frac{\partial V}{\partial t} = 4\pi r^2 v. \tag{10}$$

Substituting (10) into equation (9) for a given flow velocity and replacing r with D for conduit diameter results in the following expression:

$$\Delta p = \frac{32\eta l v}{D^2}. \tag{11}$$

A kinematic viscosity of 20×10^{-6} m^2/s (20 cSt) is typical for uncured polydimethylsiloxane fluid, and uncured silicone has a density of 950 kg/m^3 at room temperature (295 K) [20]. In this case of the silicones used in this work (Silikonfabrik SF00), the density is somewhat higher at 1060 kg/m^3, and the dynamic viscosity is about 1.5 Pas.

A volumetric flow rate of 16 ml/min (actual measured data) equates to $2.7E-7$ m^3/s. A diameter D of 1.5 mm has a cross-sectional area of $1.77E-6$ m^2 giving a flow velocity of 0.15 m/s. A conduit length l is given as 10 mm.

Applying actual dimensions to expression (11) yields a pressure gradient of 32000 N/m^3 (0.32 bar). This represents a manageable pressure drop given the screw power provided (60 W). Consequently, the mechanical/hydraulic power required is approximately 8.5 mW.

Entering the derived values into formula (12) yields the Reynolds factor Re:

$$\mathrm{Re} = \frac{\rho v D}{\eta}. \tag{12}$$

Such a very low Reynolds number (0.16) confirms the prerequisite of laminar flow. As a consequence, the

Hagen–Poiseuille's law, which applies only to laminar flow, can be used.

7. Conveying the Material

Conveying the material in a conventional smooth tube extruder is achieved by frictional forces between the material particles and the cylinder wall and/or screw surfaces together with the particles themselves. If this friction is zero, the material slides along the cylinder wall and simply rotates with the screw without forward movement. Conversely, if the material adheres too strongly to the cylinder wall, this impedes the axial conveying of the material [21, 22]. Therefore, the screw rotation conveys the material against a resistance which depends on the dimensions of the cylinder, the viscosity of the mixture, the mass flow rate, the screw geometry, and other boundary conditions. As already mentioned, the viscosity of PDMS depends on shear rate and temperature. Conveying against resistance causes an increase in cylinder pressure which is necessary for optimal homogenization. Due to the material adhering to the cylinder wall as well as to the screw and moving relative to each other, a drag flow occurs from the inlet to the nozzle. This is proportional to the rotational speed and the thread depth (h). In general, this is independent of the flow properties of the medium [23]. In addition to the drag flow, the backup flow or pressure flow is described, which results from the pressure buildup caused by unequal flow rates of different screw sections together with a mass backlog in front of the extrusion head. Depending on the pressure profile along the extruder, this is equal to or opposite to the drag flow. Another flow component is the leakage flow. This describes the part which flows through the gap between the extruder screw and the cylinder wall. Since this gap is extremely narrow, the material is subjected to high shear stress at this position. The result of these complex flow conditions is a thorough mixing and homogenization of the material in the extruder. The superimposition of the flows results in a pressure maximum. The position of this pressure maximum depends on the screw geometry, the process parameters (e.g., speed and temperature), and the material behavior [24].

Two additional flow parameters must be considered with the flow of viscoelastic liquids-shear flow and expansion flow. Assuming laminar flow in the gap, in accordance with (12), the medium is subjected to a shear load due to the flow process. If the wall adhesion according to Stokes [24] and the maximum flow velocity are included, a velocity gradient forms in the flow channel, the shear velocity. The maximum shear velocity is near the conduit wall; therefore the shear stress is at its highest in this area. This shear stress results in friction between the polymer chains and a subsequent dissipation of thermal energy. Consequently, most of the heat is generated along the conduit wall. At the flow front, the medium cools, resulting in a deflection of molecules from the center of the flow channel to the outside in the direction of the wall. This flow process, known as the expansion flow, leads to an alignment and expansion of the volume element. Both the expansion flow and shear flow effects influence the molecular orientation in the extruded 3D print mixture. In the case of synthetic materials containing fibres, particles, or other fillers, the flow effects also have an impact on the orientation of the additives.

8. Individual Components of the 3D Printing System

The entire 3D printing system, illustrated in Figure 2 and subsequently described in more detail, employs an extruder developed during this work.

8.1. Dosage Application. A special dosing unit is required for automatic dosage of the 2-component silicones and respective additives. It is necessary that the products be dispensed precisely per unit volume by the dosing system regardless of volume and mixing ratio. The most important parameters, the mixed dosage volume and the dosage cycle time, must be adjusted and monitored by a suitable control system. In addition, a distinction is made between static mixing cartridges, which are suitable for a variety of applications and dynamic dosing systems.

8.2. Pump System. The pumping system (modified Ismatec Ecoline ISM1078B peristaltic pump) transfers the 2 uncured liquid silicone components A and B from their respective tanks to the hopper. Component A contains the base-forming material, and component B contains the catalyst. Optionally, it is possible to include particulate additives to one or other of the components. In addition, inhibitors, catalysts, or silicone oil may also be injected into the hopper.

8.3. Extruder. The main focus of this work concerns the development of the extruder shown in Figure 2. The extruder contains the hopper, screw conveyor, and degassing valve and forms the core of the silicone (MAP or EAP) 3D printing process. In the hopper, component A and component B are merged for the first time. The hopper is designed to allow the components to come into contact quickly. The volume of the hopper is maintained as small as possible, but the feed rate must be large enough to fill the conduit within a short time.

As illustrated in Figure 3, the individual components of the screw conveyor are mounted on a stainless steel shaft, which is driven by using a microcontroller- (Arduino-) controlled stepper motor (QSH 4218-35-10-027). To ensure that the individual components are rotated, they are connected to the shaft by a feather key connection. In addition to the feather key, there are both a shaft seal and a radial deep groove ball bearing on each side of the shaft. The function of the shaft seals is to protect the interior from external influences and to prevent leakage of the mixture. Radial deep groove ball bearings smoothly transmit torque at high rotational velocities whilst absorbing axial and radial forces [25, 26].

The continuous material transport and pressure buildup required to overcome the ejection resistance is carried out by a two-stage rotating screw mounted on the stainless steel shaft by a feather key connection. The height and width of the threads are the same, screw 1 has a smaller pitch in order to generate a higher pressure and homogenize components

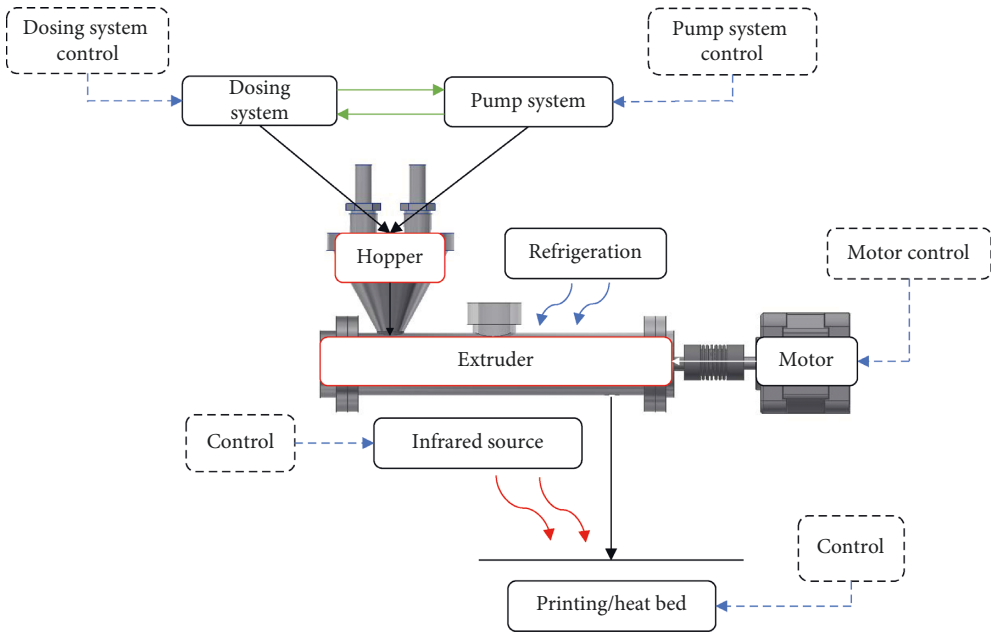

Figure 2: Overview of the entire 3D printing system.

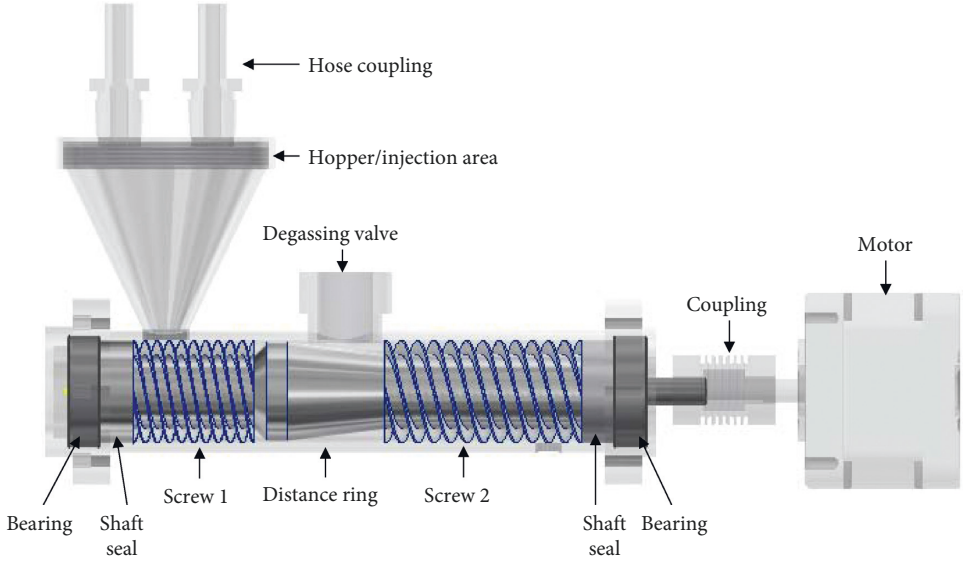

Figure 3: Final extruder prototype, screw conveyor.

A and B, whereas the pitch of screw 2 is slightly larger as it is primarily intended for material transport.

The distance ring shown in Figure 3, comprising a spacer ring and a subsequent conical cylinder, is also mounted on the shaft by means of a feather key connection. The throttle gap is now formed by the distance (about 0.8 mm) between the spacer ring and the conduit wall. The two component mixture is conveyed under high pressure through the narrow throttle gap. In the immediately following degassing part, the distance to the conduit wall decreases and the material expands. As a result, gaseous products are released and allowed to escape through a degassing valve (FLUXX® SABEU F17 degassing valve; TRAKETCH® membrane). By mixing the two components A and B, a certain amount of air is inevitably introduced into the silicone mass. The degassing valve membranes are hydrophobic and oleophobic. They are resistant to moisture, including liquids with very low surface tension, and therefore remain permanently breathable. With the help of the drip slope, liquids can drain off immediately after contact, thus maintaining the membrane contamination free and air-permeable. Since the pressure at the point of the throttle gap is higher than that in the remaining cylinder, it is necessary to seal the gap between screw 1 and the conical spacing ring, for which an O-ring is employed. This should prevent the mixture of the two components from passing through the gap to the shaft. The extrusion head is in the form of detachable cannulas and their retainer making it possible to change nozzle sizes easily and quickly after each 3D print.

With the exception of the shaft, all components are made from aluminium whose good thermal conductivity ensures

better heat transfer than other metals such as brass and stainless steel. Other materials may also be suitable, but it is important that none are ferromagnetic in cases where MAP production is concerned.

8.4. Printing/Heat Bed. The printing bed, shown in Figure 2, comprises a high-quality square (210 mm × 210 mm) flexible self-adhesive silicone heating mat. In conventional 3D printing, the heat generated serves to increase adhesion which results in improved printing results. In addition, for 3D printing of silicones, the heating mat is indispensable to the crosslinking process. As already mentioned, the vulcanization speed of addition-curing 2-component silicone systems (RTV-2) is exclusively controlled by temperature. A rough rule of thumb is to halve the pot life time for each temperature rise ΔT of 7°C (Wacker Silicones), as given in the following equation:

$$\tau_c = \frac{1}{1.1^{\Delta T}}. \quad (13)$$

The reverse applies analogously to cooling. Incipient vulcanization is noticeable by an increase in viscosity. As an alternative, infrared radiation may be employed. This has the advantage of making layer-by-layer control of the crosslinking process possible.

8.5. Maintenance. Nonvulcanized residues of RTV-2 silicones can easily be removed with solvents such as gasoline or acetone. Already vulcanized material can only be removed by mechanical action. It is therefore advisable to wash through with one of the two components (A or B) after completion of the 3D printing process, prior to cleaning with acetone.

8.6. Key Data of the Extruder. The most important extruder data are the containment volume, conveying volume, and conveying velocity. The following data are dependent on different factors and are merely intended as a guideline. If the volume of the screw conveyor is subtracted from the volume of the cylinder, the capacity of the extruder (in this case 10.9 ml) is obtained. The conveying volume describes the transported volume per revolution which reaches the printing bed through the cannula. This, in turn indicates that the 3.0 mm pitch b and the 2.85 mm thread depth of screw 2 are decisive. The conveying volume may be calculated according to the following equation:

$$V_c = 2\pi rhb = 429.8\,\text{mm}^3, \quad (14)$$

where $h = 2.85$ mm and $r = 8$ mm.

The conveying capacity depends on the pumping system and stepper motor rotor speed. Typically a pump rotor speed between 3.5 and 350 rpm, adjustable in 1% steps, suffices. Resulting flow rates lie between 13 ml/min and 4600 ml/min. In the above design, the 40 rpm rotational velocity of the stepper motor results in a conveying capacity of approximately 16 ml/min.

8.7. Preliminary Performance. The current design is presently in operation and preliminary results show significant improvements over traditional manual or machine mixing. In addition to mechanical testing (rheometry, indentation, etc.), X-ray tomography can be used to evaluate 3D-printed objects. Where particle additives are included in the 3D printing process, the shedding of particles during cavity ascension during the degassing process leads to the formation of ring structures. The deliberate introduction of cavities can have advantages [11], though in most cases such inhomogeneities are a major problem.

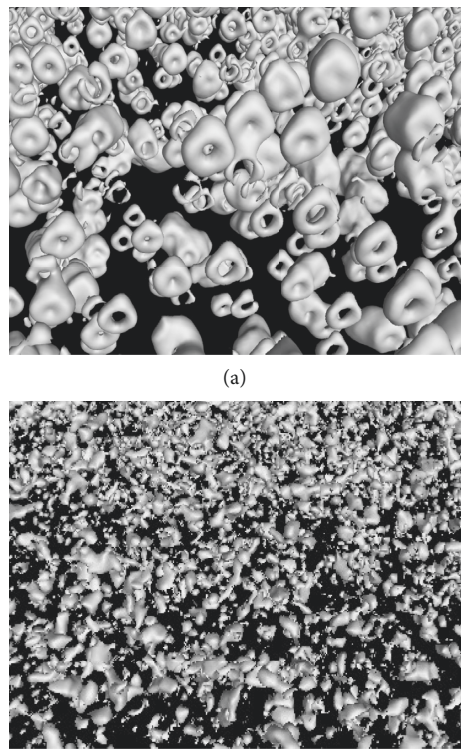

(a)

(b)

Figure 4: X-ray tomographs of MAP (a) containing rings and (b) ring-free MAP.

Figure 4 shows 3D X-ray tomographic images of magnetoactive polymers containing 3wt.% CIP, containing rings resulting from cavity ascension (Figure 4(a)) and ring free due to the absence of cavities (Figure 4(b)).

9. Conclusions

A miniature extruder capable of cavity-free mixing of addition-curing RTV-2 silicones, with or without particulate additives, has been developed, built, and successfully tested. The extruder is capable of direct inclusion in automated 3D and 6D printing systems and overcomes many of the problems associated with conventional mixing, such as cavity inclusion, sedimentation of particulate, limited printing time, and postprocess intensive cleaning. Design parameters are given, and the basic formulas necessary for relevant rheological calculations are derived.

Additional components are required for full integration into a 3D printing system, but these are individual to specific 3D printer designs. The necessary materials are readily

available making the miniature extruder a cost-effective component of any 3D printing system. Although this work deals specifically with silicones, the miniature extruder is extremely versatile and applicable to the extrusion of other two part materials.

Data Availability

The data used to support the findings of this study are available from the corresponding author upon request.

Conflicts of Interest

The authors declare that there are no conflicts of interest regarding the publication of this paper.

Acknowledgments

The authors would like to express their thanks to the German Research (DFG) for financial support within the SPP1681 research program. In addition, the authors would like to express their gratitude to SABEU for the FLUXX® devolatilizing valve with its TRAKETCH® membrane, the workshops of OTH/University Regensburg for the completion of the extruder, and Sigma-Aldrich for material samples.

References

[1] L. Raddatz, J. Austerjost, and S. Beutel, "3D-Druck: chancen, möglichkeiten, risiken," *Chemie in Unserer Zeit*, vol. 52, no. 1, pp. 42–50, 2018.

[2] W. Sommer, A. Schlenker, and C.-D. Lange-Schönbeck, *Faszination 3D-Druck: Alles zum Drucken, Scannen, Modellieren*, Markt+Technik Verlag GmbH, Burgthann, Germany, 2016.

[3] M. V. Gandhi and B. S. Thompson, *Smart Materials and Structures*, Springer, London, UK, 1992.

[4] H. Hanselka and J. Nuffer, *Intelligent Materials: Principles-Applications-Trends*, Springer, Berlin, Germany, 2009.

[5] W. Cao, H. H. Cudney, and R. Waser, "Smart materials and structures," *Proceedings of the National Academy of Sciences*, vol. 96, no. 15, pp. 8330-8331, 1999.

[6] N. Prem, *Spectroscopic Analysis of Magnetoactive Polymers (MAPs)–Master Project Report 1*, Technical University of Applied Science Regensburg, Regensburg, Germany, 2017.

[7] P. Saxena, J.-P. Pelteret, and P. Steinmann, "Modelling of iron-filled magneto-active polymers with a dispersed chain-like microstructure," *European Journal of Mechanics-A/Solids*, vol. 50, pp. 132–151, 2015.

[8] G. J. Monkman, D. Sindersberger, A. Diermeier, and N. Prem, "The magnetoactive electret," *Smart Materials and Structures*, vol. 26, no. 7, article 075010, 2017.

[9] N. Prem, J. C. Vega, V. Böhm, D. Sindersberger, G. J. Monkman, and K. Zimmermann, "Properties of Polydimethylsiloxane and magnetoactive polymers with electroconductive particles," *Macromolecular Chemistry and Physics*, vol. 219, no. 18, article 1800222, 2018.

[10] D. Sindersberger, A. Diermeier, N. Prem, and G. J. Monkman, "Printing of hybrid magneto active polymers with 6 degrees of freedom," *Materials Today Communications*, vol. 15, pp. 269–274, 2018.

[11] D. Sindersberger, N. Prem, and G. J. Monkman, "Structure formation in low concentration magnetoactive polymers," *AIP Advances*, vol. 9, article 035322, 2019.

[12] E. Forster, M. Mayer, R. Rabindranath et al., "Surface control and characterization of ultra soft magneto-active polymers (MAP)," in *EuroEAP, First international conference on Electromechanically Active Polymer (EAP) transducers & artificial muscles*, Pisa, Italy, June 2011.

[13] N. Bosq, N. Guigo, J. Persello, and N. Sbirrazzuoli, "Melt and glass crystallization of PDMS and PDMS silica nanocomposites," *Physical Chemistry Chemical Physics*, vol. 16, no. 17, pp. 7830–7840, 2014.

[14] J. E. Mark, *Physical Properties of Polymers Handbook*, Springer, New York, NY, USA, 2nd edition, 2007.

[15] W. Niedermeier, J. Fröhlich, and H.-D. Luginsland, "Reinforcement mechanism in the rubber matrix by active fillers-raw materials and applications," *KGK Kautschuk Gummi Kunststoffe*, vol. 55, pp. 7-8, 2002.

[16] M. Mayer, R. Rabindranath, J. Börner et al., "Ultra-soft PDMS-based magnetoactive elastomers as dynamic cell culture substrata," *PLoS One*, vol. 8, no. 10, Article ID e76196,, 2013.

[17] P. Pelz, *Rheologie der Kautschukmischungen, Elastomer Werkstoffe*, Freudenberg Forschungsdienste KG, Weinheim, Germany, 2001.

[18] T. Schröder, *Rheologie der Kunststoffe: Theorie und Praxis*, Carl Hanser GmbH, Munich, Germany, 2018.

[19] H. Schade and F. Kameier, *Strömungslehre*, de Gruyter, Berlin, Germany, 4th edition, 2013, http://www.degruyter.com/doi/book/10.1515/9783110292237.

[20] C. Roberts, A. Graham, M. Nemer, L. Phinney, R. Garcia, and E. Stirrup, "Physical properties of low-molecular weight Polydimethylsiloxane fluids," Sandia Report SAND2017-1242, Sandia National Laboratories, Livermore, CA, USA, 2017.

[21] O.-H. Elhami, "Charakterisierung eines einschneckenextruders zur herstellung von pyrolysekoks-pasten," Diplomarbeit, Karlsruhe Institute of Technology (KIT), Karlsruhe, Germany, 2013.

[22] P. G. Lafleur and B. Vergnes, *Polymer Extrusion*, John Wiley & Sons, Inc., London, UK, 2014.

[23] H. Potente and S. Kleineheisman, "Ermittlung der tribologischen Materialkennwerte von thermoplastischen Kunststoffgranulaten," *Kunststofftechnik-Heft*, vol. 5, pp. S201–S219, 2009.

[24] H. Greif, A. Limper, and G. Fattmann, *Technologie der Extrusion: Lern- und Arbeitsbuch für die Aus- und Weiterbildung*, Hanser, Munich, Germany, 2nd edition, 2018.

[25] DIN 625-1/2011-04 Industrienorm, *Rolling Bearings-Radial Deep Groove Ball Bearings–Part 1: Single Row*, German Institute for Standardization, Berlin, Germany, 2011.

[26] SKF Gruppe, "Wälzlager–document PUB BU/P1 10000/2 DE," 2014, http://www.skf.com/binary/78-121486/0Walzlager-10000_2-DE.pdf.